System-level effects of CO_2 and RuBisCO concentration on carbon isotope fractionation

Amanda K. Garcia[1‡], Mateusz Kedzior[1‡], Arnaud Taton[2], Meng Li[3], Jodi N. Young[3] and Betül Kaçar [1,4*]

[1]Department of Molecular and Cellular Biology, University of Arizona, Tucson, AZ

[2]Division of Biological Sciences, University of California San Diego, La Jolla, CA

[3]School of Oceanography, University of Washington, Seattle, WA

[4]Lunar and Planetary Laboratory, Department of Planetary Sciences, University of Arizona, Tucson, AZ

[‡]These authors contributed equally to this work.

*For correspondence: betul@arizona.edu

KEYWORDS

carbon fixation, carbon isotope fractionation, RuBisCO, biosignatures, cyanobacteria

ABSTRACT

Carbon isotope biosignatures preserved in the Precambrian geologic record are primarily interpreted to reflect ancient cyanobacterial carbon fixation catalyzed by Form I RuBisCO enzymes. The average range of isotopic biosignatures generally follows that produced by extant cyanobacteria. However, this observation is difficult to reconcile with several environmental (e.g., temperature, pH, and CO_2 concentrations), molecular and physiological factors that likely would have differed during the Precambrian and can produce fractionation variability in contemporary organisms that meets or exceeds that observed in the geologic record. To test a range of genetic and environmental factors that may have impacted ancient carbon isotope biosignatures, we engineered a mutant strain of the model cyanobacterium *Synechococcus elongatus* PCC 7942 that overexpresses RuBisCO and characterized the resultant physiological and isotope fractionation effects. We specifically investigated how both increased atmospheric CO_2 concentrations and RuBisCO regulation influence cell growth, oxygen evolution rate, and carbon isotope fractionation in cyanobacteria. We found that >2% CO_2 increases the growth rate of wild-type and mutant strains, and that the pool of active RuBisCO enzyme increases with increased expression. At elevated CO_2, carbon isotope discrimination (ε_p) is increased by ~8‰, whereas RuBisCO overexpression does not significantly affect isotopic discrimination at all tested CO_2 concentrations. Our results show that understanding the environmental factors that impact RuBisCO regulation, physiology, and evolution is crucial for reconciling microbially driven carbon isotope fractionation with the geologic record of organic and inorganic carbon isotope signatures.

IMPORTANCE

Carbon isotope biosignatures preserved in the geologic record are interpreted to reflect the long-term evolution of microbial carbon fixation and provide the earliest evidence of life on Earth. RuBisCO enzymes, distinctive and early-evolved catalysts that fix atmospheric CO_2, have likely been responsible for the bulk of primary productivity through Earth history. Thus, a comprehensive understanding of the molecular, physiological, environmental, and evolutionary factors that influence the isotopic discrimination of cyanobacteria that utilize RuBisCO is essential for the interpretation of ancient isotopic biosignatures. For example, the vastly different atmospheric CO_2 levels that characterized the Precambrian may have influenced the expression and regulation of the ancient RuBisCO protein complex. These observations underscore the need to consider how a broader range of environmental conditions and subcellular processes may have shaped isotopic discrimination over geologic time. In this study, we establish a cyanobacterial metabolic-engineering strategy that can test such hypotheses and offer insights into the biogeochemical record of life.

INTRODUCTION

The conserved microbial metabolic pathways that drive global biogeochemistry emerged on Earth billions of years ago, the evolution of which has both shaped and been shaped by large-scale environmental transitions (Falkowski, Fenchel, & Delong, 2008; Knoll, Bergmann, & Strauss, 2016; Lyons, Fike, & Zerkle, 2015). These microbial processes have left distinct signatures that evidence biological activity billions of years in the past. Of these, the oldest and most extensive signature of biological activity on Earth is the deviation in stable carbon isotopic compositions ($^{13}C/^{12}C$, expressed as $\delta^{13}C$) between preserved inorganic and organic carbon, interpreted to reflect the isotopic discrimination of ancient biological carbon fixation (Des Marais, 2001; Krissansen-Totton, Buick, & Catling, 2015; Lloyd et al., 2020; Schidlowski, 2001). These deviations are primarily shaped by enzymes that preferentially assimilate the lighter ^{12}C isotope from inorganic carbon sources. Carbon biosignatures preserved in the geologic record therefore reflect the long-term evolution of these enzyme-mediated processes and their hosts' physiologies.

The RuBisCO enzyme (ribulose 1,5-bisphosphate (RuBP) carboxylase/oxygenase) catalyzes the reduction of inorganic CO_2 as the initial step of carbon assimilation into organic biomass via the Calvin-Benson-Bassham (CBB) cycle (Erb & Zarzycki, 2018; Nisbet et al., 2007; Tcherkez, Farquhar, & Andrews, 2006). RuBisCO is one of the most abundant proteins on Earth (Bar-On & Milo, 2019; Ellis, 1979; Raven, 2013), and its presence in photoautotrophic organisms, including early-evolved cyanobacteria, suggests that this enzyme has played a significant role in primary production for much of Earth history (Hamilton, Bryant, & Macalady, 2016; Schirrmeister, Sanchez-Baracaldo, & Wacey, 2016; Schopf, 2011). Thus, the isotopic fractionation behavior of RuBisCO is also thought to have primarily constrained Precambrian carbon isotope signatures

preserved in the geologic record (Garcia, Cavanaugh, & Kacar, 2021; Schidlowski, 1988). Though there exist multiple forms of RuBisCO, the known range of Form I RuBisCO isotopic fraction (ε ≈ 20-30‰) (R. D. Guy, Fogel, & Berry, 1993; Scott et al., 2007; von Caemmerer, Tazoe, Evans, & Whitney, 2014) — the form utilized by extant cyanobacteria and responsible for the bulk of modern primary production (Field, 1998) — is largely consistent with the ~25‰ mean deviation between preserved inorganic and organic carbon isotopic compositions across geologic time (Des Marais, 2001; Garcia et al., 2021; Havig, Hamilton, Bachan, & Kump, 2017; Krissansen-Totton et al., 2015; Lloyd et al., 2020; Schidlowski, 2001).

RuBisCO primarily shapes the generation of distinct carbon isotopic biosignatures associated with CBB-utilizing organisms. Nonetheless the carbon isotopic composition of bulk photoautotrophic biomass often deviates from values obtained for purified RuBisCO. This discrepancy might be attributable to several intracellular physiological and metabolic features that additionally shift the isotopic composition of organism biomass. These include the activation of carbon-concentrating mechanisms such as the partitioning of RuBisCO into carboxysomes (Hurley, Wing, Jasper, Hill, & Cameron, 2021; Laws, Popp, Cassar, & Tanimoto, 2002; Price, Badger, Woodger, & Long, 2008; Raven, Cockell, & De La Rocha, 2008), the diffusive transport of CO_2 (Hayes, 1993; Rau, Riebesell, & Wolf-Gladrow, 1996), and intermediary carbon-fixing steps (Eungrasamee, Miao, Incharoensakdi, Lindblad, & Jantaro, 2019; H. I. Guy & Evans, 1996; Hayes, 1993; Rothschild & DesMarais, 1989). Further, studies show that photosynthetic carbon isotope discrimination (ε_p) may vary due to environmental factors and cellular physiological responses, including temperature (Deleens, Treichel, & O'Leary, 1985; Wong & Sackett, 1978), pH (Hinga, Arthur, Pilson, & Whitaker, 1994; Roeske & O'Leary, 1984), growth rate (Bidigare et al., 1997; Laws, Bidigare, &

Popp, 1997), and CO_2 concentration (Eichner, Thoms, Kranz, & Rost, 2015; Freeman & Hayes, 1992; Hinga et al., 1994; Hurley et al., 2021; Schubert & Jahren, 2012; Wilkes, Lee, McClelland, Rickaby, & Pearson, 2018). These variations indicate a compelling need to comprehensively characterize both internal and external factors that can affect isotope fractionation, though the study of each tend to be siloed in biological and geobiological fields, respectively.

An aspect of photoautotrophic isotopic discrimination that has not been thoroughly investigated is how variable RuBisCO expression can influence host organism growth parameters and the isotopic composition of assimilated biomass. RuBisCO expression has been shown to be CO_2-sensitive (Gesch et al., 2003; Onizuka et al., 2002; Sengupta, Sunder, Sohoni, & Wangikar, 2019). This observation is particularly important, considering that atmospheric CO_2 concentrations exceeded present day levels by more than an order of magnitude for much of Earth history (between ~0.001 and 0.1 bar CO_2 through the Precambrian (Catling & Zahnle, 2020)) and that the RuBisCO catalytic efficiency itself is sensitive to the atmospheric CO_2/O_2 levels (Erb & Zarzycki, 2018; Kacar, Hanson-Smith, Adam, & Boekelheide, 2017; Poudel et al., 2020; Riebesell, Revill, Holdsworth, & Volkman, 2000; Schubert & Jahren, 2012; Scott et al., 2007; Tcherkez et al., 2006; Wilkes et al., 2018). Thus, interpretation of the carbon isotope record should take into account the coupled influence of CO_2 concentration and RuBisCO expression in generating isotopic biosignatures and shaping ancient primary productivity.

To investigate the interplay between RuBisCO expression and CO_2 concentrations on cyanobacterial fitness and carbon isotopic discrimination, we generated a genetic system to manipulate the expression levels of RuBisCO in the model organism *Synechococcus elongatus*

126 PCC 7942 (hereafter *S. elongatus*). *S. elongatus* is a naturally competent obligate photoautotroph
127 that utilizes Form I RuBisCO to fix carbon (Bonfil et al., 1998; Gabay, Lieman-Hurwitz, Hassidim,
128 Ronen-Tarazi, & Kaplan, 1998; Maeda, Price, Badger, Enomoto, & Omata, 2000; Omata, Gohta,
129 Takahashi, Harano, & Maeda, 2001; Taton et al., 2020; Tchernov et al., 2001). Specifically, we
130 engineered the *S. elongatus* genome with an additional copy of the RuBisCO operon in a
131 chromosomal neutral site to overexpress RuBisCO and permit genetic manipulation of the
132 RuBisCO operon for future studies. We confirmed proper assembly of the overexpressed RuBisCO
133 complex and its catalytic activity in the engineered strain. Then, to assess whether physiological
134 and subcellular parameters and varying CO_2 concentrations modulate carbon isotopic
135 discrimination in cyanobacteria, we determined growth rate, photosynthetic oxygen evolution rate,
136 and $^{13}C/^{12}C$ discrimination of the engineered strain in comparison to wild-type *S. elongatus*. Our
137 results suggest that increased CO_2 concentrations result in significantly faster growth in
138 cyanobacteria and increase the magnitude of isotopic discrimination. On the other hand, we show
139 that changing cellular RuBisCO levels do not significantly alter carbon isotope discrimination.
140

141 **RESULTS**

142 **A second copy of the *rbc* operon results in increased amount of active RuBisCO**

143 The RuBisCO Form I enzyme in *S. elongatus* is encoded by an operon that includes a CO_2-
144 sensitive promoter region (Sengupta et al., 2019) as well as the structural *rbcL* (large subunit) and
145 *rbcS* (small subunit) genes (Vijayan, Jain, & O'Shea, 2011). We designed *S. elongatus* strain Syn02
146 that harbors the native *rbc* operon and a second copy inserted in the chromosome neutral site 2
147 (NS2), a site that permits genetic modification without additional indirect phenotypic impact
148 (Andersson et al., 2000; Clerico, Ditty, & Golden, 2007) (**Fig. 1**). Syn02 was contructed by

149 transforming wild-type (WT) *S. elongatus* with plasmid pSyn02 carrying the *rbc* operon and
150 homologous regions directing recombination at NS2 (**Table 1**). Additionally, we generated a
151 control strain Syn01 whereby RuBisCO is provided solely by an engineered *rbc* operon at its NS2
152 site.
153
154 We evaluated whether the additional copy of the *rbc* operon in strain Syn02 resulted in RuBisCO
155 overexpression by quantifying transcription of the *rbcL* and *purK* (located downstream of *rbcL* in
156 the operon) genes by quantitative reverse-transcription PCR (RT-qPCR). Transcripts were
157 quantified and normalized to those of *secA* and *ppc* reference genes (Hood, Higgins, Flamholz,
158 Nichols, & Savage, 2016; Luo et al., 2019; Szekeres, Sicora, Dragoş, & Drugă, 2014). We found
159 that the level of *rbcL* transcript in Syn02 increased by at least 2-fold relative to WT across all
160 tested CO_2 concentrations and growth phases, and as high as ~14-fold in air ($p < 0.01$; **Fig. 2A,**
161 **Fig. S1A**). In addition, we found that *rbcL* expression increased by >5-fold at elevated CO_2
162 concentrations relative to ambient air ($p < 0.001$; **Fig. 2B, Fig. S1B).** Expression of *purK* in Syn02
163 increased by >2-fold at 2% and 5% CO_2 relative to WT, but decreased by ~0.5-fold in air (**Fig.**
164 **S1C**).
165
166 To determine *rbcL* overexpression at the protein-level, we quantified RbcL protein from crude cell
167 lysates by Western blot using rabbit anti-RbcL antibody (see **Materials and Methods**). In
168 agreement with RuBisCO overexpression indicated by the RT-qPCR results, densitometric
169 analyses revealed a mean ~2 to 4-fold increase of RbcL protein in Syn02 relative to WT across all
170 tested CO_2 concentrations ($p < 0.01$; **Fig. 2C**). Finally, we confirmed proper assembly of the large
171 (L) and small (S) subunits into the RuBisCO L_8S_8 complex in Syn02 as well as the Syn01 control

strain by native protein electrophoresis and detection by anti-RbcL antibody. We found a ~3-fold increase in assembled RuBisCO protein for Syn02 and ~2-fold increase for Syn01 relative to WT for cultures grown in 2% CO_2 (**Fig. 2D**).

Finally, we tested whether or not RuBisCO overexpression in Syn02 resulted in an increased amount of active RuBisCO by determining the total carboxylase activity of cell lysates. Enzyme activity was evaluated by an *in vitro* spectrophotometric coupled-enzyme assay that links carboxylase activity to NADH oxidation, reported as the RuBP consumption rate normalized to total soluble protein content (Kubien, Brown, & Kane, 2011). We measured a mean ~0.8-fold ($p < 0.01$) increase in Syn02 lysate RuBisCO activity relative to WT (**Fig. 2E**). No significant difference in activity was detected between Syn01 and WT cultures.

RuBisCO overexpression does not strongly influence growth rate or photosynthetic activity

We cultured WT and Syn02 *S. elongatus* strains in order to determine the influence of Syn02 RuBisCO overexpression on growth rate. Cultures were continuously sparged with ambient air, as well as 2% and 5% CO_2, with daily optical density measurements at 750 nm (OD_{750}) as described in **Materials and Methods**. WT and Syn02 both exhibited ~2.5-fold faster growth rates under 2% and 5% CO_2 compared to ambient air ($p < 0.001$; **Fig. 2A; Table 2**). Syn02 exhibited a slight ~0.1-fold increase in growth rate in ambient air relative to WT ($p < 0.05$). No difference in growth rate was observed between the two strains under 2% and 5% CO_2. The carrying capacity (maximum cell density measured at OD_{750} across the total growth period) for cultures varied between different atmospheric conditions, with a maximum carrying capacity of $OD_{750} \approx 8.4$ reached under 2% CO_2. No significant difference in carrying capacity was found between WT and

Syn02 cultures grown under the same atmospheric conditions. To determine the degree to which sparging impacted growth, we repeated the growth experiments without sparging. Minimal differences were again observed between WT and Syn02 across different CO_2 concentrations (**Table S1**).

To further test for differences in photosynthetic activities between the WT and Syn02 strains, we measured their oxygen evolution rates. After brief incubation in the dark, culture samples were exposed to saturated light in an oxygen electrode chamber to detect increased levels of molecular oxygen. Oxygen evolution rates were normalized to chlorophyll *a* concentrations, following Zavrel et al. (Zavrel, Sinetova, & Červený, 2015). We did not observe a significant difference in mean oxygen evolution rate between WT and Syn02 (342 ± 26 $O_2 \cdot h^{-1} \cdot \mu g^{-1}$ chlorophyll *a* and 362 ± 26 $O_2 \cdot h^{-1} \cdot \mu g^{-1}$ chlorophyll *a,* respectively) (**Table 2**).

CO_2 concentration impacts *S. elongatus* $^{13}C/^{12}C$ fractionation

We tested both the influence of RuBisCO overexpression and CO_2 concentration on the magnitude of $^{13}C/^{12}C$ isotopic discrimination in *S. elongatus,* which was assessed by measuring the $^{13}C/^{12}C$ composition of biomass ($\delta^{13}C_{biomass}$). The isotopic discrimination associated with photosynthetic CO_2 fixation (ε_p) was then calculated from measured $\delta^{13}C_{biomass}$ and a reference $\delta^{13}C_{CO2}$ value (8.4 ‰; (Keeling et al., 2017)), as described in **Materials and Methods**. We observed that increased CO_2 concentration increases the magnitude of *S. elongatus* $^{13}C/^{12}C$ discrimination. Mean ε_p values for *S. elongatus* strains grown in ambient air were ~10‰ (**Fig. 4A**). At 2% and 5% CO_2, ε_p values were ~7-9‰ greater than those for cultures grown in air, with mean values ranging between ~17‰ to 20‰ ($p < 0.001$). Mean ε_p values were similar for WT and Syn02 strains most tested CO_2

conditions, with the exception of 5% CO2, where a significant but slight difference in ε_p values was detected (18.95‰ and 18.62‰ for WT and Syn02, respectively; $p < 0.01$). These results demonstrate that RuBisCO overexpression in Syn02 does not strongly impact cyanobacterial $^{13}C/^{12}C$ discrimination.

DISCUSSION

In this study, we developed an integrative approach to investigate the coupled impact of CO_2 levels and RuBisCO expression on cyanobacterial growth, fitness and carbon isotope discrimination. We tested whether the overexpression of RuBisCO influences *S. elongatus* growth, physiology and carbon isotope fractionation at different CO_2 atmosphere concentrations by generating an engineered *S. elongatus* strain Syn02 that harbors a second copy of the *rbc* operon at NS2.

Our transcriptional analyses indicate that *S. elongatus* strain Syn02 overexpresses RuBisCO relative to WT at all tested CO_2 concentrations (ambient air, 2%, and 5% CO_2) (**Fig. 2A, Fig. 2C**). In addition, we found that *rbcL* transcript levels increase for all strains at elevated CO_2 levels relative to air (**Fig. 2B**). This result is in agreement with a previous study reporting a regulatory element in the *S. elongatus* PCC 7942 *rbcL* operon that regulates the expression of RbcL with increasing CO_2 (Sengupta et al., 2019). We found that the magnitude of increased *rbcL* transcription between Syn02 and WT was lower at elevated CO_2 (**Fig. 2A**). For example, in air, *rbcL* transcript levels in Syn02 were ~14-fold greater than in WT, but in 2% CO_2, only a ~2-fold increase was observed. These results indicate that, whereas RuBisCO expression is impacted by CO_2 concentration, other physiological factors such as the translation efficiency or expression of

other ancillary crucial proteins may ~~may~~ be limiting RuBisCO expression and dampen the effects of an additional copy of the *rbc* operon in Syn02.

Protein-level analyses indicate that increased *rbc* transcription in Syn02 relative to WT does result in increased cellular RuBisCO concentration. The magnitude of this increase is relatively constant (~2-3 fold) across different CO_2 concentrations (**Fig. 2C**). These results are supported by a ~2-fold increase in assembled RuBisCO L_8S_8 protein in Syn02 relative to WT (**Fig. 3A**). However, the ~0.8-fold increase in carboxylase activity of Syn02 cell lysate relative to that of WT was not directly proportional to the increase in protein amount observed by Western blot analyses, suggesting that not all overexpressed RuBisCO was catalytically active (**Fig. 3B**). Previous studies showed overexpression of RuBisCO in cyanobacteria generally produces an increased pool of active carboxylase (Atsumi, Higashide, & Liao, 2009; Iwaki et al., 2006; Lechno-Yossef et al., 2020; Liang & Lindblad, 2017). However, it is possible that not all overexpressed RuBisCO may be properly assembled, e.g., due to limited chaperonin GroEL/ES, which is known to be involved in RuBisCO folding (Hayer-Hartl, 2017; Liu et al., 2010). Altogether, our findings suggest that additional physiological constraints may be limiting RuBisCO expression beyond transcription. The exact mechanism of the regulation we observed in our experiments await further characterization.

Various culture conditions including pH, temperature, CO_2 concentration, and light intensity may substantially affect the growth characteristics of cyanobacteria, and thus have the potential to influence isotopic discrimination (Kuan, Duff, Posarac, & Bi, 2015; Rillema, MacCready, & Vecchiarelli, 2020; Ungerer, Lin, Chen, & Pakrasi, 2018; Yu et al., 2015). The influence of genetic

263 factors, including the regulation of RuBisCO expression on cyanobacterial fitness, is less well
264 known. Previous studies targeting the correlation between RuBisCO overexpression and fitness in
265 cyanobacteria have yielded mixed results. For instance, faster growth rates and oxygen evolution
266 rates were observed for an engineered *Synechocystis* PCC 6803 strain that overexpresses RuBisCO
267 (Liang & Lindblad, 2017), as well as in *S. elongatus* upon co-overexpression of its
268 phosphoribulokinase (Kanno, Carroll, & Atsumi, 2017). However, in *Synechococcus* sp. PCC
269 7002, the overexpression of RuBisCO did not alter growth rate (De Porcellinis et al., 2018). The
270 impact of RuBisCO upregulation on cyanobacterial growth appears to be species/strain-specific.
271 Our data shows that RuBisCO overexpression in *S. elongatus* PCC 7942 strain Syn02 results in a
272 minor increase in growth rate in ambient air relative to WT, and no significant difference was
273 observed at elevated CO_2 levels, nor for oxygen evolution rates. Under ambient environmental
274 conditions, RuBisCO has a relatively high baseline level of expression in cyanobacteria (V.
275 Vijayan, I. H. Jain, & E. K. O'Shea, 2011), perhaps explaining why increased expression does not
276 significantly improve fitness. Our results indicate that further study is needed to fully understand
277 the coupled interaction of different environmental conditions and genetic backgrounds in
278 determining cyanobacterial fitness.
279
280 Another important aspect to consider is the degree to which genetic regulation and background
281 may impact system-level isotope fractionation in cyanobacteria. Understanding the connection
282 between genetics and biogeochemistry, though often overlooked, can augment interpretation of
283 isotopic biosignatures in deep time. We measured the carbon isotopic composition of
284 cyanobacterial biomass ($\delta^{13}C_{biomass}$) and photosynthetic carbon isotopic discrimination (ε_p) in WT
285 and Syn02 cultured under a range of CO_2 concentrations. The increased expression and activity of

RuBisCO in Syn02 apparently neither changed the availability of carbon isotopes in the enzyme's vicinity nor altered the performance of other cellular modules contributing to carbon isotope discrimination. $\delta^{13}C_{biomass}$ and ε_p values were comparable for WT and Syn02 grown at all tested CO_2 concentrations (**Fig. 4**).

Our results show that at both 2% and 5% CO_2, ε_p values were increased by ~7-9‰ for WT and Syn02 strains relative to air. Theoretically, under high CO_2 concentrations, the intrinsic kinetic isotope effect of RuBisCO is expressed and maximizes ε_p (Bidigare et al., 1997; Hayes, 1993; Schubert & Jahren, 2012; Wilkes et al., 2018). Under these conditions, other cellular modules, such as carbon concentrating mechanisms capable of discriminating carbon isotopes, produce negligible impact on net carbon discrimination at the organismal level (Hurley et al., 2021; Laws et al., 2002). The positive relationship between CO_2 concentration and carbon isotope fractionation has been observed empirically for a variety of autotrophs (Freeman & Hayes, 1992; Hinga et al., 1994; Schubert & Jahren, 2012; Wilkes et al., 2018), including for cyanobacteria in particular (Eichner et al., 2015; Hurley et al., 2021). Other studies showed that photoautotrophs that grew under a lower pH, and thus a higher proportion of CO_2, also exhibited higher carbon fractionation (Mizutani & Wada, 1982; Roeske & O'Leary, 1984; Wang, Yeager, & Lu, 2016; Yoshioka, 1997). The ε_p values observed under high inorganic carbon availability fall within the range of 17-20‰ (**Fig. 4B**), which follows the range known for Form I RuBisCO (R. D. Guy et al., 1993; McNevin, Badger, Kane, & Farquhar, 2006; Scott et al., 2007).

Based on the data generated here, we speculate that, in addition to environmental factors such as CO_2 concentrations, RuBisCO variation at the gene and enzymatic level, rather than its

overexpression and regulation, may be a more significant determinant of the isotopic composition of produced biosignatures. Less well-characterized RuBisCO forms (i.e., Forms IC, ID, and II) that are found in proteobacteria and marine phytoplankton can exhibit significantly smaller fractionation factors than that observed for forms associated with land plants and cyanobacteria (Boller, Thomas, Cavanaugh, & Scott, 2011; Robinson et al., 2003; Thomas et al., 2019). The full diversity of RuBisCO isotopic fractionation requires further study~~,~~. Our results underscore that the integration of synthetic biology, metabolic engineering and geochemistry can offer new insights into the study and interpretation of biogeochemical reservoirs at the global scale. Further work needs to be performed to elucidate how the intracellular factors impact metabolisms responsible for carbon isotope fractionation under ancient transitions in environmental conditions. A deeper understanding of the impact of the RuBisCO regulation and the environmental factors on the resulting organismal behavior is essential to establish the extent to which the RuBisCO isotope fractionation properties can be correlated with evidence for biological activity in the Earth's deep past.

ACKNOWLEDGEMENTS

This work was supported by the National Science Foundation Emerging Frontiers Program Award No. 1724090 (BK), NASA Early Career Faculty (ECF) Award No. 80NSSC19K1617 (BK.), NASA Postdoctoral Fellowship (AKG.), Simons Foundation Early Career Award No. 561645 (JNY and ML), and National Institute of General Medical Sciences of the National Institutes of Health award number R01GM118815 (AT, to James W. Golden at the University of California-San Diego). We sincerely thank Bob Blankenship, Zach Adam, Katie McGrath and the members

of the Kaçar Lab for their thoughtful comments and suggestions; Sky Dominguez and the University of California-Davis Stable Isotope Facility for the assistance.

MATERIALS AND METHODS

Cyanobacterial growth and maintenance

S. elongatus PCC 7942 strains were cultured in BG-11 medium (Rippka, Deruelles, Waterbury, Herdman, & Stanier, 1979) as liquid cultures or on agar plates (1.5% (w/v) agar and 1 mM $Na_2S_2O_3 \cdot 5H_2O$). For recombinant strains, liquid and solid media were supplemented with appropriate antibiotics: 2 $\mu g \cdot ml^{-1}$ Spectinomycin (Sp) plus 2 $\mu g \cdot ml^{-1}$ Streptomycin (Sm), 5 $\mu g \cdot ml^{-1}$ Kanamycin (Km). The cyanobacterial growth was measured at optical density at 750 nm (OD_{750}).

The strains were archived at -80 °C in 15% (v/v) glycerol. The 2-ml vials were rapidly thawed and inoculated in liquid BG-11 (supplemented with antibiotics as needed). Cultures were shaken at 120 rpm at 30 °C under continuous low illumination of 45 µmol photon$\cdot m^{-2} \cdot s^{-1}$, and ambient air, until they reached an OD_{750} between 0.4 and 0.6. These cultures were then used to inoculate fresh cultures that were grown using similar conditions but under moderate illumination of 80 µmol photon$\cdot m^{-2} \cdot s^{-1}$ and sparged at selected CO_2 concentrations (ambient air, 2%, or 5% CO_2; cultures were also grown without sparging to assess differences in growth rate; **Table S1**). When cultures reached an OD_{750} of ~7 to 7.5, they were sampled for subsequent experiments as described below (cultures were also sampled at an earlier OD_{750} of 0.5-1.5 for additional RT-qPCR experiments, see below; **Fig. S1**).

354 **Genetic engineering of cyanobacteria**

355 A recombinant strains of *S. elongatus* was constructed by natural transformation using standard
356 protocols (Clerico et al., 2007) and the plasmids and methods described below (**Table 1**) . To
357 construct the plasmid pSyn02, pAM4937 was digested with *Swa*I to release the *ccdB* toxic gene
358 and produce a plasmid backbone that contains the pBR322 *E. coli* origin of replication, the base
359 of mobilization site for conjugal transfer, the *aph1* gene conferring kanamycin resistance, and
360 sequences for homologous recombination into *S. elongatus* chromosome at NS2. The *rbc* operon
361 was amplified from *S. elongatus* PCC 7942 gDNA with primers F01 and R01 (**Table S2**)
362 containing 20-nucleotide sequences that overlap with pAM4937 backbone. The resulting DNA
363 fragments were assembled using the GeneArt™ Seamless Cloning and Assembly Kit (Invitrogen,
364 Cat. No. A13288). pSyn02 was used to insert the *rbc* operon into NS2 of the wild type genome in
365 the strain PCC 7942 through homologous recombination to create the strain of *S. elongatus*, Syn02,
366 carrying two copies of the *rbc* operon. Plasmid pSyn-01 was constructed by using two primer pairs
367 F02/R02 and F03/R03 (**Table S2**), 1) to amplify a fragment of pAM4951 that contains the *E. coli*
368 origin of replication and the site for conjugal transfer, and 2) to amplify the *aadA* gene conferring
369 spectinomycin/streptomycin resistance. Native *rbc* operon flanking sequences were amplified
370 from the *S. elongatus* PCC 7942 gDNA with the primer pairs F04/R04 and F05/R05 (**Table S2**)
371 containing 20-nucleotide sequences that overlap with the pAM4951 fragments.
372
373 Transformation was carried out after growing the WT strain in liquid culture at 30 °C with shaking
374 (120 rpm) and a light intensity of 80 µmol photon·m^{-2}·s^{-1} until an OD_{750} ~0.7. The cells were
375 prepared for transformation according to the protocol by Clerico et al. (2007) and plated on BG-
376 11 agar containing the appropriate antibiotic(s) for recovery. Subsequently, the colonies were

picked using sterile pipette tips, patched onto BG-11 agar containing the appropriate antibiotic(s), and further incubated to ensure complete chromosome segregation (i.e., incorporation of the *trans*-gene into all chromosomes). The patched transformants were screened using colony PCR using the primers F06/R06 and F07/R07 and the genotypes of the engineered strains were confirmed by Sanger sequencing using the primers F08/R08 **(Fig. S2, Table S2**)

Extraction of total RNA and proteins

Cultures were collected during the exponential growth phase. Cells were pelleted by centrifugation at 4,700 × g for 10 min at room temperature and resuspended in 10 mL of TE buffer (10 mM Tris, pH 8.0, 1 mM EDTA). To prepare the crude cell lysate, 8 mL of the cell suspension were pelleted by centrifugation at 4,700 × g for 10 min at room temperature, resuspended in 500 µL of hot (pre-warmed to 95 °C) TE buffer supplemented with 1% (w/v) SDS and incubated at 95 °C for 10 min. Then, the mixture was sonicated at 40% amplitude for 3 × 10 sec with 10 sec intervals, and the cell debris centrifuged at 17,000 × g for 10 min at room temperature. The supernatant was collected and stored at -80 °C. Total RNA was extracted from the remaining 2 mL of the cell suspension using the RNeasy® Protect Bacteria Mini Kit (QIAGEN, Cat. No. 74524) following the manufacturer instructions.

Analysis of *rbc* operon expression by RT-qPCR

Total RNA was quantified with the NanoDrop spectrophotometer and 1 µg of RNA was treated with the amplification grade deoxyribonuclease I (Invitrogen, Cat. No. 18068-015). 10 µL of DNase I-treated RNA was then used in reverse transcription (RT) performed with the SuperScript™ IV First-Strand Synthesis System (Invitrogen, Cat. No. 18091050). The four pairs

of qPCR primers (listed in **Table S2**) were designed with Primer3Plus (http://www.bioinformatics.nl/cgi-bin/primer3plus/primer3plus.cgi). Both reference genes have previously been shown to be stably expressed under diverse conditions in *S. elongatus* (Luo et al., 2019). The quality of cDNA and primer specificity was assessed by PCR using cDNA templates (RT positive reactions), RT negative controls, and the qPCR primers. The analysis of gene expression levels was performed in the real-time thermal cycler qTOWER^3 G (Analytik Jena AG), equipped with the software qPCRsoft, using the cycles: 50 °C/2 min, 95 °C/2 min, 40 × (95 °C/15 sec, 60 °C/1 min). The relative expression of the *rbc* operon genes (*rbcL* and *purK*) was calculated as the average fold change normalized to reference genes using the delta-delta Ct method. The experiment was carried out using three biological replicates and three technical replicates.

Analysis of RbcL protein by Western blot

Total protein concentration in the crude cell lysates was measured using the Pierce™ BCA Protein Assay Kit (Thermo Scientific, Cat. No. 23225). The lysates were loaded in the amount of 5 µg of total protein in Laemmli sample buffer onto a 6% (v/v) polyacrylamide stacking gel. Proteins were electrophoresed in a 12% polyacrylamide resolving gel in TGS buffer and blotted in transfer buffer onto a PVDF membrane. Total protein load in each sample was visualized by Revert™ 700 Total Protein Stain (LI-COR Biosciences, Cat. No. 926-11011) and used for the RbcL signal normalization. Detection of RbcL was performed by overnight incubation of the membrane at 4 °C with rabbit anti-RbcL antibody (Agrisera, Cat. No. AS03 037), 1:5000 in TBST with 5% non-fat milk, followed by one-hour incubation at room temperature with IRDye® 800CW goat anti-rabbit IgG secondary antibody (LI-COR Biosciences, Cat. No. 926-32211), 1:20,000 in Intercept® (TBS) blocking buffer (LI-COR Biosciences, Cat. No. 927-60001) with 0.1% (v/v) Tween-20 and

0.01% (w/v) SDS. Both the total protein load and the amount of RbcL in each sample were documented with Odyssey® Fc Imaging System (LI-COR Biosciences, Cat. No. 2800-03) at the near-infrared detection mode. The images were acquired using Image Studio™ software. The densitometric analysis of RbcL signal intensity, normalized to total protein load, was performed with Quantity One® software (Bio-Rad) for six biological replicates. The amount of RbcL produced by each replicate of the Syn02 strain culture was compared to the averaged level of RbcL in the WT PCC 7942 replicate cultures and expressed as the averaged percent of RbcL synthesized by the WT strain.

Assembly of RuBisCO subunits

Assembly of the RuBisCO large and small subunits into a hexadecameric complex in each strain was evaluated by native gel electrophoresis and immunodetection of the RuBisCO complexes. Samples were collected during the exponential growh phase. Cells were pelleted by centrifugation at 4,700 × g for 10 min at room temperature and resuspended in 400 µL of native lysis buffer (50 mM Tris, pH 8.0, 150 mM NaCl, 1 mM EDTA, 10% (v/v) glycerol) supplemented with 5 mM DTT, 100 µg/mL lysozyme from chicken egg white, and 1% (v/v) Halt™ Protease Inhibitor Cocktail (Thermo Scientific, Cat. No. 78430). The cell suspensions were incubated at 30 °C for 15 min and subjected to five consecutive freeze-thaw cycles (10 min at -80 °C followed by 5 min at 30 °C), then were sonicated on ice for 3 minutes at 30% amplitude (2-sec on/off intervals), centrifuged at 17,000 × g for 15 min at 4 °C. The concentration of total soluble proteins in the lysates was determined with Pierce™ BCA Protein Assay Kit. The lysates were adjusted to 5 µg of total soluble proteins in native sample buffer and then loaded onto a 4-20% Mini-PROTEAN® TGX™ Precast Protein Gel (Bio-Rad, Cat. No. 4561094). Protein electrophoreses were performed

in TG buffer (60 mM Tris, 192 mM glycine) at 100 V for 4 h at 4 °C and blotted in transfer buffer (48 mM Tris, pH 9.2, 39 mM glycine, 0.04% (w/v) SDS) onto a nitrocellulose membrane. After three 10-min washes in wash buffer (48 mM Tris, pH 9.2, 39 mM glycine, 20% (v/v) methanol), total protein load in each sample was visualized by Revert™ 700 Total Protein Stain and used for the normalization of RuBisCO complex quantity. Immunodetection of the RuBisCO complex was performed with the same primary and secondary antibodies that were used to analyze the level of RbcL, as described above.

Catalytic activity of RuBisCO

The activity of RuBisCO in cyanobacterial lysates was measured using a spectrophotometric coupled-enzyme assay that links this activity with the rate of NADH oxidation (Kubien et al., 2011). The cyanobacterial strains were cultured, collected, and pelleted as described above. The pellets were resuspended in 1 mL of ice-cold lysis buffer (50 mM EPPS, 1 mM EDTA, 2 mM DTT, pH 8.0) and transferred into 2 mL screw-capped tubes with Lysing Matrix B (MP Biomedical) for lysis by bead beating using FastPrep-24™ 5G bead beater (MP Biomedical) with 4 m/sec for 10 sec, followed by 2-min incubation on ice, repeated six times. The cell lysates were transferred to new Eppendorf tubes to remove the beads and unbroken cells and to pellet the thylakoid membrane by centrifugation at 10,000 × g for 1 min and at 20,000 × g for 30 min at 4 °C, sequentially. The resulting clear supernatants containing cytosolic soluble proteins, including phycobiliproteins and RuBisCO, were used to determine protein concentration by Pierce™ BCA Protein Assay Kit and to measure RuBisCO activity by employing an assay adapted from Kubien et al. (2011). The assay buffer (100 mM HEPES, 25 mM $MgCl_2$, 1 mM EDTA, pH 7.6) was used considering the high Michaelis constant for CO_2 (K_C) for cyanobacterial RuBisCO. 20 µL of cell

lysates were preincubated in the assay mix (with 5 mM $NaHCO_3$) at 25 °C for activation before initiating the reaction by adding synthesized ribulose 1,5-bisphosphate (RuBP) according to Kane et al. (Kane, Wilkin, Portis, & John Andrews, 1998). The absorbance at 340 nm was monitored using the Synergy H1 plate reader (BioTek). RuBisCO activity was reported as RuBP consumption rate normalized to total soluble protein content. The assay was performed for three biological replicates.

Cyanobacterial growth measurements

OD_{750} values were plotted as a function of time and analyzed in R with the Growthcurver package. Growth curve data was fitted to the standard form of the logistic equation to calculate growth parameters including growth rate, doubling time, and carrying capacity (Sprouffske & Wagner, 2016). Each strain was grown in triplicate for every condition.

Photosynthetic oxygen evolution rate

S. elongatus strain photosynthetic activity was assayed using a Clark-type oxygen electrode chamber to measure the level of molecular oxygen produced in cyanobacterial cultures. Cells were grown in 50 mL of BG-11 at 30 °C, illumination of 80 µmol photon·m^{-2}·s^{-1}, shaking at 120 rpm, in ambient air, and with culture sparging. The samples were collected from triplicate cultures during the exponential growth phase, pelleted by centrifugation at 4,700 × g for 10 min at room temperature, and resuspended in fresh BG-11 to an OD_{750} of ~1.0. Concentration of chlorophyll *a* (for normalization) was measured following the protocol by Zavrel et al. (Zavrel et al., 2015). The remaining suspension was incubated in the dark for 20 min with gentle agitation. Samples from each suspension, prepared in three technical replicates, were analyzed in an oxygen electrode

chamber under saturated light, using the Oxygraph+ System (Hansatech Instruments) equipped with the OxyTrace+ software. Oxygen evolution rate was monitored for 10 min and expressed as nanomoles of molecular oxygen evolved per hour per microgram of chlorophyll *a*.

Carbon isotope fractionation in bulk cyanobacterial biomass

The bacteria were pelleted by centrifugation at 4,700 × g for 10 min at room temperature, washed in 10 mL of 10 mM NaCl. The bacteria were resuspended in 1 mL of 10 mM NaCl and transferred to Eppendorf tubes. After centrifugation at 4,700 × g for 10 min at room temperature, the supernatants were completely removed, the pellets were dried in opened tubes in a laboratory oven at 50 °C for 2 days, and the resultant dried biomass samples were transferred into tin capsules.

The carbon isotope composition of bulk biomass ($\delta^{13}C_{biomass}$) samples was determined at the UC Davis Stable Isotope Facility. $\delta^{13}C_{biomass}$ was analyzed using a PDZ Europa ANCA-GSL elemental analyzer interfaced to a PDZ Europa 20-20 isotope ratio mass spectrometer (Sercon Ltd.). The carbon isotopic composition values were reported relative to the Vienna PeeDee Belemnite standard (V-PDB):

$$\delta^{13}C_{sample} = \left(\frac{^{13}C / ^{12}C_{sample}}{^{13}C / ^{12}C_{V-PDB}} - 1 \right) \times 1000$$

The carbon isotope fractionation associated with photosynthetic CO_2 fixation (ε_p) was calculated relative to a reference $\delta^{13}C_{CO2}$ value (-8.4‰; (Keeling et al., 2017)) according to Freeman and Hayes (1992):

$$\varepsilon_p = \frac{\delta^{13}C_{CO_2} - \delta^{13}C_{biomass}}{1 + \delta^{13}C_{biomass} / 1000}$$

514

515 **Statistical analyses**

516 Results for experimental analyses were presented as the mean and the sample standard deviation
517 (SD) values of at least three independent experiments. Statistical significance was analyzed swith
518 the two-tailed *t*-test. The unpaired sample *t*-test assuming equal variances was used to compare the
519 values obtained for different cyanobacterial strains and the paired sample *t*-test was used to
520 compare the values for the same strain at different experimental conditions.

521

REFERENCES

Andersson, C. R., Tsinoremas, N. F., Shelton, J., Lebedeva, N. V., Yarrow, J., Min, H., & Golden, S. S. (2000). Application of bioluminescence to the study of circadian rhythms in cyanobacteria. *Methods Enzymol, 305*, 527-542.

Atsumi, S., Higashide, W., & Liao, J. C. (2009). Direct photosynthetic recycling of carbon dioxide to isobutyraldehyde. *Nat Biotechnol, 27*(12), 1177-1180. doi:10.1038/nbt.1586

Bar-On, Y. M., & Milo, R. (2019). The global mass and average rate of rubisco. *Proc Natl Acad Sci USA, 10*, 4738-4743. doi:10.1073/pnas.1816654116

Bidigare, R. R., Fluegge, A., Freeman, K. H., Hanson, K. L., Hayes, J. M., Hollander, D., . . . Wakeham, S. G. (1997). Consistent fractionation of ^{13}C in nature and in the laboratory: growth-rate effects in some haptophyte algae. *Global Biogeochem Cycles, 11*(2), 279-292. doi:10.1029/96gb03939

Boller, A. J., Thomas, P. J., Cavanaugh, C. M., & Scott, K. M. (2011). Low stable carbon isotope fractionation by coccolithophore RubisCO. *Geochimica et Cosmochimica Acta, 75*(22), 7200-7207. doi:10.1016/j.gca.2011.08.031

Bonfil, D. J., Ronen-Tarazi, M., Sultemeyer, D., Lieman-Hurwitz, J., Schatz, D., & Kaplan, A. (1998). A putative HCO3- transporter in the cyanobacterium Synechococcus sp. strain PCC 7942. *FEBS Lett, 430*(3), 236-240.

Catling, D. C., & Zahnle, K. J. (2020). The Archean atmosphere. *Science Advances, 6*(9). doi:10.1126/sciadv.aax1420

Clerico, E. M., Ditty, J. L., & Golden, S. S. (2007). Specialized techniques for site-directed mutagenesis in cyanobacteria. *Methods Mol Biol, 362*, 155-171. doi:10.1007/978-1-59745-257-1_11

De Porcellinis, A. J., Norgaard, H., Brey, L. M. F., Erstad, S. M., Jones, P. R., Heazlewood, J. L., & Sakuragi, Y. (2018). Overexpression of bifunctional fructose-1,6-bisphosphatase/sedoheptulose-1,7-bisphosphatase leads to enhanced photosynthesis and global reprogramming of carbon metabolism in Synechococcus sp. PCC 7002. *Metab Eng, 47*, 170-183. doi:10.1016/j.ymben.2018.03.001

Deleens, E., Treichel, I., & O'Leary, M. H. (1985). Temperature dependence of carbon isotope fractionation in CAM plants. *Plant Physiology, 79*(1), 202-206. doi:10.1104/pp.79.1.202

Des Marais, D. J. (2001). Isotopic evolution of the biogeochemical carbon cycle during the Precambrian. *Reviews in Mineralogy and Geochemistry, 43*(1), 555-578. doi:10.2138/gsrmg.43.1.555

Eichner, M., Thoms, S., Kranz, S. A., & Rost, B. (2015). Cellular inorganic carbon fluxes in Trichodesmium: a combined approach using measurements and modelling. *J Exp Bot, 66*(3), 749-759. doi:10.1093/jxb/eru427

Ellis, R. J. (1979). The most abundant protein in the world. *Trends in Biochemical Sciences, 4*(11), 241-244.

Erb, T. J., & Zarzycki, J. (2018). A short history of RubisCO: the rise and fall (?) of Nature's predominant CO_2 fixing enzyme. *Curr Opin Biotechnol, 49*, 100-107. doi:10.1016/j.copbio.2017.07.017

Eungrasamee, K., Miao, R., Incharoensakdi, A., Lindblad, P., & Jantaro, S. (2019). Improved lipid production via fatty acid biosynthesis and free fatty acid recycling in engineered Synechocystis sp. PCC 6803. *Biotechnology for biofuels, 12*, 8-8. doi:10.1186/s13068-018-1349-8

567 Falkowski, P. G., Fenchel, T., & Delong, E. F. (2008). The microbial engines that drive Earth's
568 biogeochemical cycles. *Science, 320*(5879), 1034-1039. doi:10.1126/science.1153213
569 Field, C. B. (1998). Primary Production of the Biosphere: Integrating Terrestrial and Oceanic
570 Components. *Science, 281*(5374), 237-240. doi:10.1126/science.281.5374.237
571 Freeman, K. H., & Hayes, J. M. (1992). Fractionation of carbon isotopes by phytoplankton and
572 estimates of ancient CO_2 levels. *Global Biogeochemical Cycles, 6*(2), 185-198.
573 doi:10.1029/92gb00190
574 Gabay, C., Lieman-Hurwitz, J., Hassidim, M., Ronen-Tarazi, M., & Kaplan, A. (1998).
575 Modification of topA in Synechococcus sp. PCC 7942 resulted in mutants capable of
576 growing under low but not high concentration of CO2. *FEMS Microbiology Letters,*
577 *159*(2), 343-347. doi:10.1111/j.1574-6968.1998.tb12881.x
578 Garcia, A. K., Cavanaugh, C. M., & Kacar, B. (2021). The curious consistency of carbon
579 biosignatures over billions of years of Earth-life coevolution. *ISME J*.
580 doi:10.1038/s41396-021-00971-5
581 Gesch, R. W., Kang, I. H., Gallo-Meagher, M., Vu, J. C. V., Boote, K. J., H. Allen, L., & Bowes,
582 G. (2003). Rubisco expression in rice leaves is related to genotypic variation of
583 photosynthesis under elevated growth CO2 and temperature. *Plant, Cell & Environment,*
584 *26*(12), 1941-1950. doi:10.1046/j.1365-3040.2003.01110.x
585 Guy, H. I., & Evans, D. R. (1996). Function of the major synthetase subdomains of carbamyl-
586 phosphate synthetase. *J Biol Chem, 271*(23), 13762-13769. doi:10.1074/jbc.271.23.13762
587 Guy, R. D., Fogel, M. L., & Berry, J. A. (1993). Photosynthetic fractionation of the stable
588 isotopes of oxygen and carbon. *Plant Physiol, 101*(1), 37-47. doi:10.1104/pp.101.1.37

589 Hamilton, T. L., Bryant, D. A., & Macalady, J. L. (2016). The role of biology in planetary
590 evolution: cyanobacterial primary production in low-oxygen Proterozoic oceans.
591 *Environmental Microbiology, 18*(2), 325-340. doi:10.1111/1462-2920.13118
592 Havig, J. R., Hamilton, T. L., Bachan, A., & Kump, L. R. (2017). Sulfur and carbon isotopic
593 evidence for metabolic pathway evolution and a four-stepped Earth system progression
594 across the Archean and Paleoproterozoic. *Earth-Science Reviews, 174*, 1-21.
595 doi:10.1016/j.earscirev.2017.06.014
596 Hayer-Hartl, M. (2017). From chaperonins to Rubisco assembly and metabolic repair. *Protein*
597 *Science, 26*(12), 2324-2333. doi:10.1002/pro.3309
598 Hayes, J. M. (1993). Factors controlling 13C contents of sedimentary organic compounds:
599 Principles and evidence. *Marine Geology, 113*(1-2), 111-125. doi:10.1016/0025-
600 3227(93)90153-m
601 Hinga, K. R., Arthur, M. A., Pilson, M. E. Q., & Whitaker, D. (1994). Carbon isotope
602 fractionation by marine phytoplankton in culture: the effects of CO_2 concentration, pH,
603 temperature, and species. *Global Biogeochemical Cycles, 8*(1), 91-102.
604 doi:10.1029/93gb03393
605 Hood, R. D., Higgins, S. A., Flamholz, A., Nichols, R. J., & Savage, D. F. (2016). The stringent
606 response regulates adaptation to darkness in the cyanobacterium Synechococcus
607 elongatus. *Proc Natl Acad Sci U S A, 113*(33), E4867-4876.
608 doi:10.1073/pnas.1524915113
609 Hurley, S. J., Wing, B. A., Jasper, C. E., Hill, N. C., & Cameron, J. C. (2021). Carbon isotope
610 evidence for the global physiology of Proterozoic cyanobacteria. *Science Advances, 7*(2).
611 doi:10.1126/sciadv.abc8998

612 Iwaki, T., Haranoh, K., Inoue, N., Kojima, K., Satoh, R., Nishino, T., . . . Wadano, A. (2006).
613 Expression of foreign type I ribulose-1,5-bisphosphate carboxylase/ oxygenase (EC
614 4.1.1.39) stimulates photosynthesis in cyanobacterium Synechococcus PCC7942 cells.
615 *Photosynth Res, 88*(3), 287-297. doi:10.1007/s11120-006-9048-x
616 Kacar, B., Hanson-Smith, V., Adam, Z. R., & Boekelheide, N. (2017). Constraining the timing
617 of the Great Oxidation Event within the Rubisco phylogenetic tree. *Geobiology, 15*(5),
618 628-640. doi:10.1111/gbi.12243
619 Kane, H. J., Wilkin, J.-M., Portis, A. R., & John Andrews, T. (1998). Potent Inhibition of
620 Ribulose-Bisphosphate Carboxylase by an Oxidized Impurity in Ribulose-1,5-
621 Bisphosphate. *Plant Physiology, 117*(3), 1059-1069. doi:10.1104/pp.117.3.1059
622 Kanno, M., Carroll, A. L., & Atsumi, S. (2017). Global metabolic rewiring for improved CO2
623 fixation and chemical production in cyanobacteria. *Nature Communications, 8*(1), 14724.
624 doi:10.1038/ncomms14724
625 Keeling, R. F., Graven, H. D., Welp, L. R., Resplandy, L., Bi, J., Piper, S. C., . . . Meijer, H. A. J.
626 (2017). Atmospheric evidence for a global secular increase in carbon isotopic
627 discrimination of land photosynthesis. *Proc Natl Acad Sci U S A, 114*(39), 10361-10366.
628 doi:10.1073/pnas.1619240114
629 Knoll, A.H., Bergmann, K.D. and Strauss, J.V., 2016. Life: the first two billion
630 years. *Philosophical Transactions of the Royal Society B: Biological Sciences*, *371*(1707),
631 p.20150493.
632 Krissansen-Totton, J., Buick, R., & Catling, D. C. (2015). A statistical analysis of the carbon
633 isotope record from the Archean to Phanerozoic and implications for the rise of oxygen.
634 *American Journal of Science, 315*(4), 275-316. doi:10.2475/04.2015.01

635 Kuan, D., Duff, S., Posarac, D., & Bi, X. (2015). Growth optimization ofSynechococcus
636 elongatusPCC7942 in lab flasks and a 2-D photobioreactor. *The Canadian Journal of*
637 *Chemical Engineering, 93*(4), 640-647. doi:10.1002/cjce.22154
638 Kubien, D. S., Brown, C. M., & Kane, H. J. (2011). Quantifying the amount and activity of
639 Rubisco in leaves. *Methods Mol Biol, 684*, 349-362. doi:10.1007/978-1-60761-925-3_27
640 Laws, E. A., Bidigare, R. R., & Popp, B. N. (1997). Effect of growth rate and CO_2 concentration
641 on carbon isotopic fractionation by the marine diatom *Phaeodactylum tricornutum*.
642 *Limnology and Oceanography, 42*(7), 1552-1560. doi:10.4319/lo.1997.42.7.1552
643 Laws, E. A., Popp, B. N., Cassar, N., & Tanimoto, J. (2002). 13C discrimination patterns in
644 oceanic phytoplankton: likely influence of CO2 concentrating mechanisms, and
645 implications for palaeoreconstructions. *Functional Plant Biology, 29*(3).
646 doi:10.1071/pp01183
647 Lechno-Yossef, S., Rohnke, B. A., Belza, A. C. O., Melnicki, M. R., Montgomery, B. L., &
648 Kerfeld, C. A. (2020). Cyanobacterial carboxysomes contain an unique rubisco-activase-
649 like protein. *New Phytologist, 225*(2), 793-806. doi:10.1111/nph.16195
650 Liang, F., & Lindblad, P. (2017). Synechocystis PCC 6803 overexpressing RuBisCO grow faster
651 with increased photosynthesis. *Metab Eng Commun, 4*, 29-36.
652 doi:10.1016/j.meteno.2017.02.002
653 Liu, C., Young, A. L., Starling-Windhof, A., Bracher, A., Saschenbrecker, S., Rao, B. V., . . .
654 Hayer-Hartl, M. (2010). Coupled chaperone action in folding and assembly of
655 hexadecameric Rubisco. *Nature, 463*(7278), 197-202. doi:10.1038/nature08651

656 Lloyd, M. K., McClelland, H. L. O., Antler, G., Bradley, A. S., Halevy, I., Junium, C. K., . . .
657 Zerkle, A. L. (2020). The Isotopic Imprint of Life on an Evolving Planet. *Space Science*
658 *Reviews, 216*(7). doi:10.1007/s11214-020-00730-6
659 Luo, X., Li, J., Chang, T., He, H., Zhao, Y., Yang, X., . . . Xu, Y. (2019). Stable Reference Gene
660 Selection for RT-qPCR Analysis in Synechococcus elongatus PCC 7942 under Abiotic
661 Stresses. *Biomed Res Int, 2019*, 7630601. doi:10.1155/2019/7630601
662 Lyons, T. W., Fike, D. A., & Zerkle, A. (2015). Emerging Biogeochemical Views of Earth's
663 Ancient Microbial Worlds. *Elements, 11*(6), 415-421. doi:10.2113/gselements.11.6.415
664 Maeda, S., Price, G. D., Badger, M. R., Enomoto, C., & Omata, T. (2000). Bicarbonate binding
665 activity of the CmpA protein of the cyanobacterium Synechococcus sp. strain PCC 7942
666 involved in active transport of bicarbonate. *J Biol Chem, 275*(27), 20551-20555.
667 doi:10.1074/jbc.M003034200
668 McNevin, D. B., Badger, M. R., Kane, H. J., & Farquhar, G. D. (2006). Measurement of (carbon)
669 kinetic isotope effect by Rayleigh fractionation using membrane inlet mass spectrometry
670 for CO2-consuming reactions. *Functional plant biology : FPB, 33*(12), 1115-1128.
671 doi:10.1071/fp06201
672 Mizutani, H., & Wada, E. (1982). Effect of high atmospheric CO2 concentration on δ13 of algae.
673 *Origins of life, 12*(4), 377-390. doi:10.1007/BF00927070
674 Nisbet, E. G., Grassineau, N. V., Howe, C. J., Abell, P. I., Regelous, M., & Nisbet, R. E. R.
675 (2007). The age of Rubisco: the evolution of oxygenic photosynthesis. *Geobiology, 5*,
676 311-335. doi:10.1111/j.1472-4669.2007.00127.x

677 Omata, T., Gohta, S., Takahashi, Y., Harano, Y., & Maeda, S. (2001). Involvement of a CbbR
678 homolog in low CO2-induced activation of the bicarbonate transporter operon in
679 cyanobacteria. *J Bacteriol, 183*(6), 1891-1898. doi:10.1128/JB.183.6.1891-1898.2001
680 Onizuka, T., Akiyama, H., Endo, S., Kanai, S., Hirano, M., Tanaka, S., & Miyasaka, H. (2002).
681 CO2 Response Element and Corresponding trans-acting Factor of the Promoter for
682 Ribulose-1,5-bisphosphate Carboxylase/oxygenase Genes in Synechococcus sp.
683 PCC7002 Found by an Improved Electrophoretic Mobility Shift Assay. *Plant and Cell*
684 *Physiology, 43*(6), 660-667. doi:10.1093/pcp/pcf082
685 Poudel, S., Pike, D. H., Raanan, H., Mancini, J. A., Nanda, V., Rickaby, R. E. M., & Falkowski,
686 P. G. (2020). Biophysical analysis of the structural evolution of substrate specificity in
687 RuBisCO. *Proceedings of the National Academy of Sciences, 117*(48), 30451-30457.
688 doi:10.1073/pnas.2018939117
689 Price, G. D., Badger, M. R., Woodger, F. J., & Long, B. M. (2008). Advances in understanding
690 the cyanobacterial CO2-concentrating-mechanism (CCM): functional components, Ci
691 transporters, diversity, genetic regulation and prospects for engineering into plants. *J Exp*
692 *Bot, 59*(7), 1441-1461. doi:10.1093/jxb/erm112
693 Rau, G. H., Riebesell, U., & Wolf-Gladrow, D. (1996). A model of photosynthetic 13 C
694 fractionation by marine phytoplankton based on diffusive molecular CO2 uptake. *Marine*
695 *Ecology Progress Series, 133*(1/3), 275-285.
696 Raven, J. A. (2013). Rubisco: still the most abundant protein of Earth? *New Phytologist, 198*(1),
697 1-3. doi:10.1111/nph.12197

698 Raven, J. A., Cockell, C. S., & De La Rocha, C. L. (2008). The evolution of inorganic carbon
699 concentrating mechanisms in photosynthesis. *Philosophical Transactions of the Royal*
700 *Society B: Biological Sciences, 363*(1504), 2641-2650. doi:doi:10.1098/rstb.2008.0020
701 Riebesell, U., Revill, A. T., Holdsworth, D. G., & Volkman, J. K. (2000). The effects of varying
702 CO2 concentration on lipid composition and carbon isotope fractionation in Emiliania
703 huxleyi. *Geochimica et Cosmochimica Acta, 64*(24), 4179-4192. doi:10.1016/s0016-
704 7037(00)00474-9
705 Rillema, R., MacCready, J. S., & Vecchiarelli, A. G. (2020). Cyanobacterial growth and
706 morphology are influenced by carboxysome positioning and temperature.
707 doi:10.1101/2020.06.01.127845
708 Rippka, R., Deruelles, J., Waterbury, J. B., Herdman, M., & Stanier, R. Y. (1979). Generic
709 Assignments, Strain Histories and Properties of Pure Cultures of Cyanobacteria.
710 *Microbiology, 111*(1), 1-61. doi:https://doi.org/10.1099/00221287-111-1-1
711 Robinson, J. J., Scott, K. M., Swanson, S. T., O'Leary, M. H., Horken, K., Tabita, F. R., &
712 Cavanaugh, C. M. (2003). Kinetic isotope effect and characterization of form II RubisCO
713 from the chemoautotrophic endosymbionts of the hydrothermal vent tubeworm *Riftia*
714 *pachyptila*. *Limnology and Oceanography, 1*, 48-54. doi:10.4319/lo.2003.48.1.0048
715 Roeske, C. A., & O'Leary, M. H. (1984). Carbon isotope effects on the enzyme-catalysed
716 carboxylation of ribulose bisphosphate. *Biochemistry, 23*, 6275-6284.
717 Rothschild, L. J., & DesMarais, D. (1989). Stable carbon isotope fractionation in the search for
718 life on early Mars. *Adv Space Res, 9*(6), 159-165.
719 Schidlowski, M. (1988). A 3,800-Million-Year Isotopic Record of Life from Carbon in
720 Sedimentary-Rocks. *Nature, 333*(6171), 313-318. doi:DOI 10.1038/333313a0

721 Schidlowski, M. (2001). Carbon isotopes as biogeochemical recorders of life over 3.8 Ga of
722 Earth history: evolution of a concept. *Precambrian Research, 106*(1-2), 117-134. doi:Doi
723 10.1016/S0301-9268(00)00128-5
724 Schirrmeister, B. E., Sanchez-Baracaldo, P., & Wacey, D. (2016). Cyanobacterial evolution
725 during the Precambrian. *International Journal of Astrobiology, 15*(3), 187-204.
726 doi:10.1017/s1473550415000579
727 Schopf, J. W. (2011). The paleobiological record of photosynthesis. *Photosynth Res, 107*(1), 87-
728 101. doi:10.1007/s11120-010-9577-1
729 Schubert, B. A., & Jahren, A. H. (2012). The effect of atmospheric CO2 concentration on carbon
730 isotope fractionation in C3 land plants. *Geochimica et Cosmochimica Acta, 96*, 29-43.
731 doi:10.1016/j.gca.2012.08.003
732 Scott, K. M., Henn-Sax, M., Harmer, T. L., Longo, D. L., Frame, C. H., & Cavanaugh, C. M.
733 (2007). Kinetic isotope effect and biochemical characterization of form IA RubisCO from
734 the marine cyanobacterium *Prochlorococcus marinus* MIT9313. *Limnology and*
735 *Oceanography, 52*(5), 2199-2204.
736 Sengupta, A., Sunder, A. V., Sohoni, S. V., & Wangikar, P. P. (2019). Fine-Tuning Native
737 Promoters of Synechococcus elongatus PCC 7942 To Develop a Synthetic Toolbox for
738 Heterologous Protein Expression. *ACS Synth Biol, 8*(5), 1219-1223.
739 doi:10.1021/acssynbio.9b00066
740 Sprouffske, K., & Wagner, A. (2016). Growthcurver: an R package for obtaining interpretable
741 metrics from microbial growth curves. *BMC Bioinformatics, 17*, 172.
742 doi:10.1186/s12859-016-1016-7

743 Szekeres, E., Sicora, C., Dragoş, N., & Drugă, B. (2014). Selection of proper reference genes for
744 the cyanobacterium Synechococcus PCC 7002 using real-time quantitative PCR. *FEMS*
745 *Microbiol Lett, 359*(1), 102-109. doi:10.1111/1574-6968.12574
746 Taton, A., Erikson, C., Yang, Y., Rubin, B. E., Rifkin, S. A., Golden, J. W., & Golden, S. S.
747 (2020). The circadian clock and darkness control natural competence in cyanobacteria.
748 *Nat Commun, 11*(1), 1688. doi:10.1038/s41467-020-15384-9
749 Taton, A., Unglaub, F., Wright, N. E., Zeng, W. Y., Paz-Yepes, J., Brahamsha, B., . . . Golden, J.
750 W. (2014). Broad-host-range vector system for synthetic biology and biotechnology in
751 cyanobacteria. *Nucleic Acids Research, 42*(17), e136-e136. doi:10.1093/nar/gku673
752 Tcherkez, G. G., Farquhar, G. D., & Andrews, T. J. (2006). Despite slow catalysis and confused
753 substrate specificity, all ribulose bisphosphate carboxylases may be nearly perfectly
754 optimized. *Proc Natl Acad Sci U S A, 103*(19), 7246-7251. doi:10.1073/pnas.0600605103
755 Tchernov, D., Helman, Y., Keren, N., Luz, B., Ohad, I., Reinhold, L., . . . Kaplan, A. (2001).
756 Passive entry of CO2 and its energy-dependent intracellular conversion to HCO3- in
757 cyanobacteria are driven by a photosystem I-generated deltamuH+. *J Biol Chem, 276*(26),
758 23450-23455. doi:10.1074/jbc.M101973200
759 Thomas, P. J., Boller, A. J., Satagopan, S., Tabita, F. R., Cavanaugh, C. M., & Scott, K. M.
760 (2019). Isotope discrimination by form IC RubisCO from *Ralstonia eutropha* and
761 *Rhodobacter sphaeroides*, metabolically versatile members of '*Proteobacteria*' from
762 aquatic and soil habitats. *Environ Microbiol, 21*(1), 72-80. doi:10.1111/1462-2920.14423
763 Ungerer, J., Lin, P.-C., Chen, H.-Y., & Pakrasi, H. B. (2018). Adjustments to Photosystem
764 Stoichiometry and Electron Transfer Proteins Are Key to the Remarkably Fast Growth of

765 the Cyanobacterium Synechococcus elongatus UTEX 2973. *mBio, 9*(1),
766 e02327-02317. doi:10.1128/mBio.02327-17
767 Vijayan, V., Jain, I. H., & O'Shea, E. K. (2011). A high resolution map of a cyanobacterial
768 transcriptome. *Genome Biology, 12*(5), R47. doi:10.1186/gb-2011-12-5-r47
769 Vijayan, V., Jain, I. H., & O'Shea, E. K. (2011). A high resolution map of a cyanobacterial
770 transcriptome. *Genome Biol, 12*(5), R47. doi:10.1186/gb-2011-12-5-r47
771 von Caemmerer, S., Tazoe, Y., Evans, J. R., & Whitney, S. M. (2014). Exploiting
772 transplastomically modified Rubisco to rapidly measure natural diversity in its carbon
773 isotope discrimination using tuneable diode laser spectroscopy. *J Exp Bot, 65*(13), 3759-
774 3767. doi:10.1093/jxb/eru036
775 Wang, S., Yeager, K. M., & Lu, W. (2016). Carbon isotope fractionation in phytoplankton as a
776 potential proxy for pH rather than for [CO2(aq)]: Observations from a carbonate lake.
777 *Limnology and Oceanography, 61*(4), 1259-1270. doi:10.1002/lno.10289
778 Wilkes, E. B., Lee, R. B. Y., McClelland, H. L. O., Rickaby, R. E. M., & Pearson, A. (2018).
779 Carbon isotope ratios of coccolith–associated polysaccharides of *Emiliania huxleyi* as a
780 function of growth rate and CO_2 concentration. *Organic Geochemistry, 119*, 1-10.
781 doi:10.1016/j.orggeochem.2018.02.006
782 Wong, W. W., & Sackett, W. M. (1978). Fractionation of stable carbon isotopes by marine
783 phytoplankton. *Geochimica et Cosmochimica Acta, 42*(12), 1809-1815.
784 doi:10.1016/0016-7037(78)90236-3
785 Yoshioka, T. (1997). Phytoplanktonic carbon isotope fractionation: equations accounting for
786 CO2-concentrating mechanisms. *Journal of Plankton Research, 19*(10), 1455-1476.
787 doi:10.1093/plankt/19.10.1455

788 Yu, J., Liberton, M., Cliften, P. F., Head, R. D., Jacobs, J. M., Smith, R. D., . . . Pakrasi, H. B.
789 (2015). Synechococcus elongatus UTEX 2973, a fast growing cyanobacterial chassis for
790 biosynthesis using light and CO2. *Scientific Reports, 5*(1), 8132. doi:10.1038/srep08132
791 Zavrel, T., Sinetova, M. A., & Červený, J. (2015). Measurement of Chlorophyll a and
792 Carotenoids Concentration in Cyanobacteria. *Bio-protocol, 5*(9), e1467.
793 doi:10.21769/BioProtoc.1467

794

795 **TABLES**

796 **Table 1. Strains and plasmids used in this study.**

Strain or plasmid	Description/Genotype	Antibiotic resistance	Source/Reference
WT	Wild-type strain of *S. elongatus* PCC 7942	-	Susan S. Golden (UC San Diego)
pAM4937	Expression vector for *S. elongatus* PCC 7942 neutral site 2 (NS2)	Km	(Taton et al., 2014)
pSyn02	pAM4937 carrying the *rbc* operon including *rbcL*, *rbcS*, *purK,* and flanking sequences from *S. elongatus* PCC 7942 (CP000100: 1479071-1484283)	Km	This study
Syn02	*S. elongatus* PCC 7942 carrying a second copy of the *rbc* operon and flanking sequences at NS2: NS2::*aphI-rbcL-rbcS-purK*- Synpcc7942_1429-Synpcc7942_1430	Km	This study
pAM4951	Expression vector for *S. elongatus* PCC 7942 neutral site 1 (NS1)	Sp+Sm	(Taton et al., 2014)
pSyn01	Plasmid to replace *S. elongatus'* native *rbc* operon (CP000100: 1479070-	Sp+Sm	This study

	1482595) with a Sp/Sm resistance gene: Δ(*rbcL-rbcS-purK)*::*aadA*.		
Syn01	*S. elongatus* strain Syn02 with the native *rbc* operon removed: Syn02 and and Δ(*rbcL-rbcS-purK)*::*aadA*.	Km, Sp+Sm	This study

797

798

799

Table 2. Growth parameters and oxygen evolution rates of *S. elongatus* strains under varying CO_2 concentrations[a].

Strain	Atmosphere	Growth rate (h^{-1})	Carrying capacity (OD_{750})	Oxygen evolution rate nmol ($O_2 \cdot h^{-1} \cdot \mu g^{-1}$ chlorophyll *a)*
WT	Air	0.017 ± 0.001	6.79 ± 0.70	342 ± 26
	2% CO_2	0.043 ± 0.002	8.43 ± 0.53	-
	5% CO_2	0.047 ± 0.005	5.35 ± 0.28	-
Syn02	Air	0.020 ± 0.001*	7.63 ± 0.54	362 ± 26
	2% CO_2	0.046 ± 0.001	8.28 ± 0.22	-
	5% CO_2	0.040 ± 0.001	5.44 ± 0.36	-

[a]Values are means of three biological replicates ± 1 SD. Asterisks indicate *t*-test result from comparison with WT for the same atmospheric condition, * – $p < 0.05$.

805 **FIGURES**

806

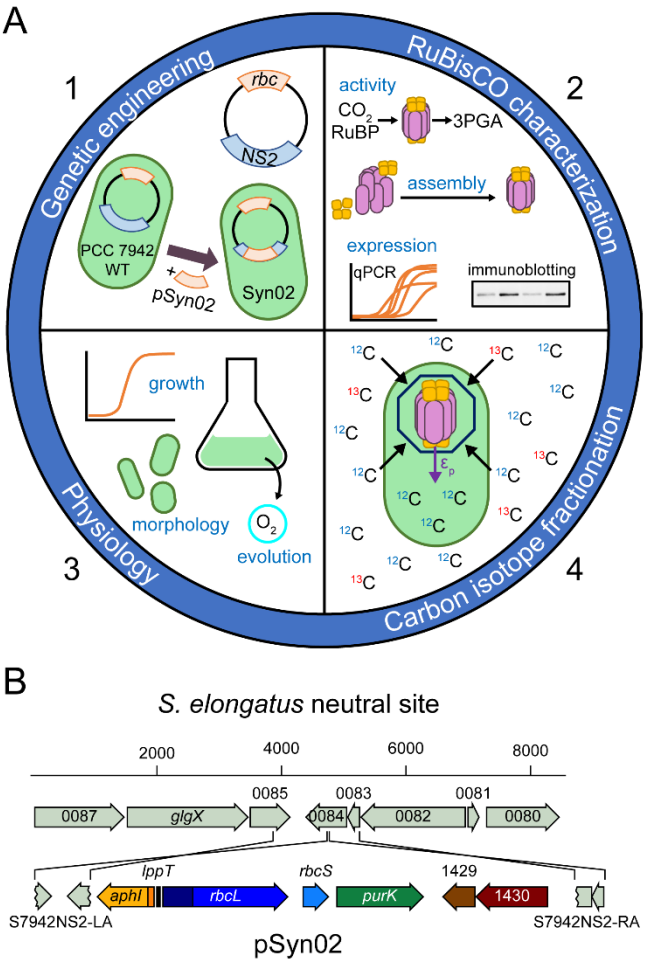

807

808 **Figure 1. Experimental strategy. A – Overall methodology. 1)** Genetic engineering: An
809 additional copy of the *rbc* operon was inserted at the chromosomal NS2 site of *S. elongatus* PCC
810 7942 to create the Syn02 strain. **2)** RuBisCO characterization was carried out by investigating (a)
811 catalytic activity, (b) assembly into a hexadecameric complex, and (c) expression at both the
812 transcript and protein levels. **3)** Physiology: *S. elongatus* WT and Syn02 strains were evaluated by
813 monitoring microbial growth characteristics, morphology, and rate of photosynthetic oxygen
814 evolution. **4**) Carbon isotope fractionation: The impact of RuBisCO overexpression on biomass
815 $\delta^{13}C$ and ε_p under varying CO_2 concentrations was assessed. **B – Map of the genetic insert in *S.***

816 ***elongatus* strain Syn02**. Plasmid pSyn02 was used to insert the *rbc* operon and the *aph1* gene
817 conferring kanamycin resistance in PCC 7942 WT NS2 to generate the Syn02 strain. Crosslines
818 indicate homologous recombination sites and scale bars show DNA fragment sizes (in bp).
819
820

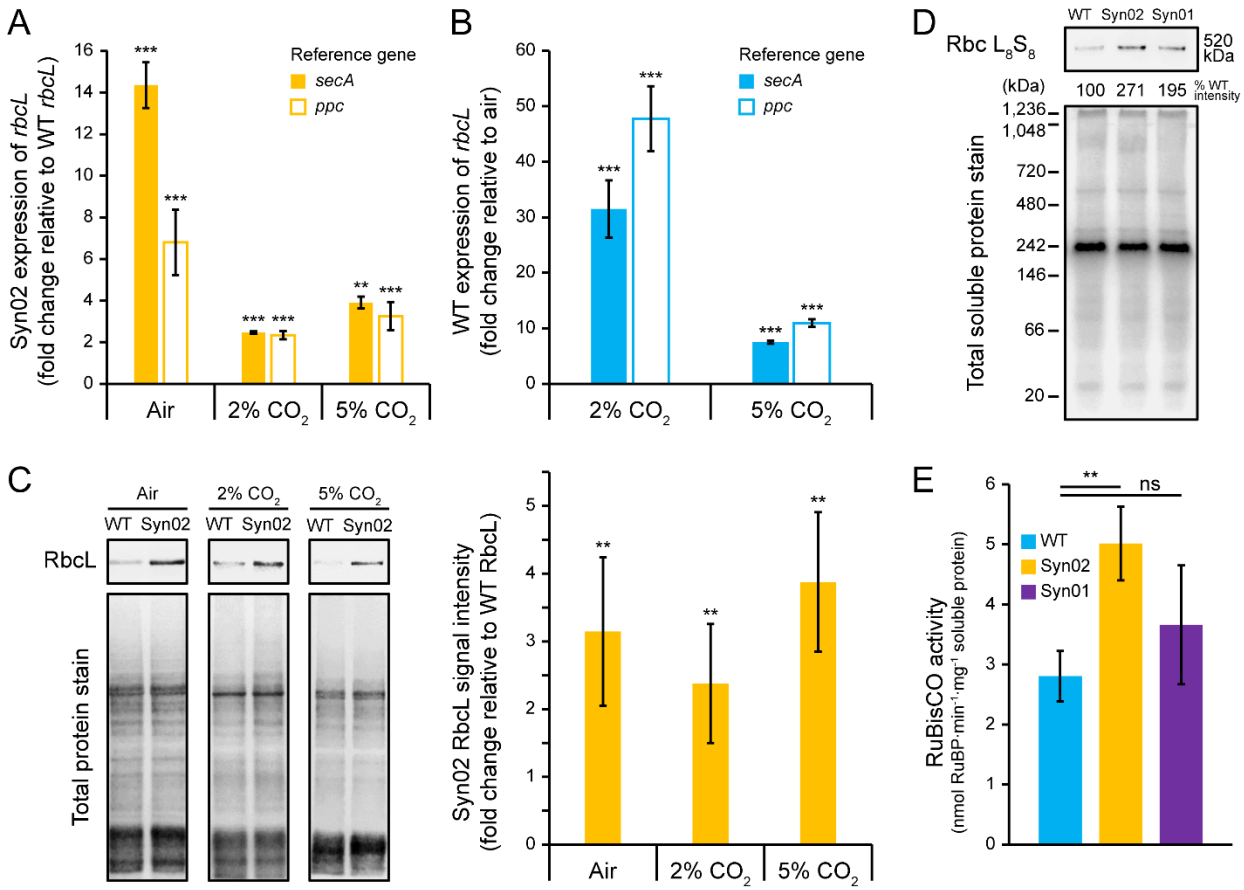

Figure 2. RuBisCO expression, assembly, and activity in *S.* elongatus strains under varying CO_2 concentrations. A – Expression of Syn02 *rbcL* relative to WT *rbcL.* Asterisks indicate *t*-test results compared to WT *rbcL* expression at the same growth condition. **B – Expression of WT *rbcL* at 2-5% CO_2 relative to ambient air.** Asterisks indicate *t*-test results compared to WT *rbcL* expression in air. **A-B –** Expression data was measured by RT-qPCR, normalized to reference genes *secA* and *ppc*. Columns represent mean fold expression for three biological replicates. **C – Immunodetection of RbcL.** (*left*) Western blot showing RbcL protein detected by anti-RuBisCO antibody and total protein stain from crude cell lysates. (*right*) RbcL percentage signal intensities were normalized to that for the total soluble protein load. Columns represent mean RbcL intensities for six biological replicates, relative to mean values for WT

cultures at the same growth condition. Asterisks indicate *t*-test results compared to WT RbcL. **D – Immunodetection of assembled RuBisCO.** Western blot showing the proper assembly of RbcL and RbcS into the L_8S_8 hexadecameric complex L_8S_8 (520 kDa), detected by anti-RbcL antibody. Rbc L_8S_8 percentage signal intensity was normalized to that for the total soluble protein load, and is shown relative to WT. **E – Lysate RuBisCO activity.** Activity was measured by the RuBP consumption rate, normalized to total soluble protein content of cell lysate. Columns represent the mean activity of three biological replicates. **A-C, E –** Asterisks indicate *t*-test results for pairwise comparison indicated by horizontal line. Error bars on all graphs indicate 1 SD. ns – not significant; ** – $p < 0.01$; *** – $p < 0.001$.

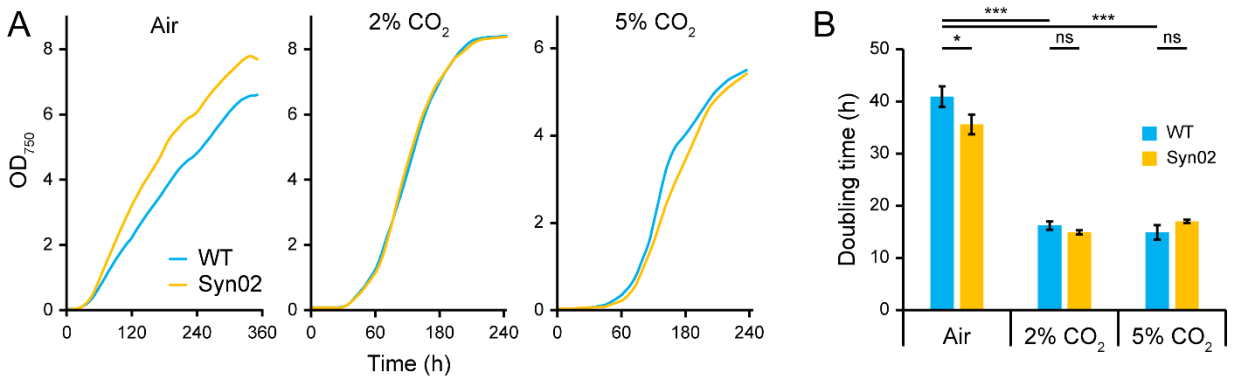

Figure 3. Growth of *S. elongatus* strains. A – Growth profiles. Cultures of each strain were maintained in ambient air or under 2% or 5% CO_2. Smoothed profiles were generated from mean optical density (measured at 750 nm, OD_{750}) values for three replicate cultures per growth condition. **B – Doubling times.** Columns represent the mean doubling time of three replicates. Error bars on all graphs indicate 1 SD, and asterisks indicate *t*-test results for pairwise comparisons indicated by horizontal lines. ns – not significant; * – $p < 0.05$; *** – $p < 0.001$.

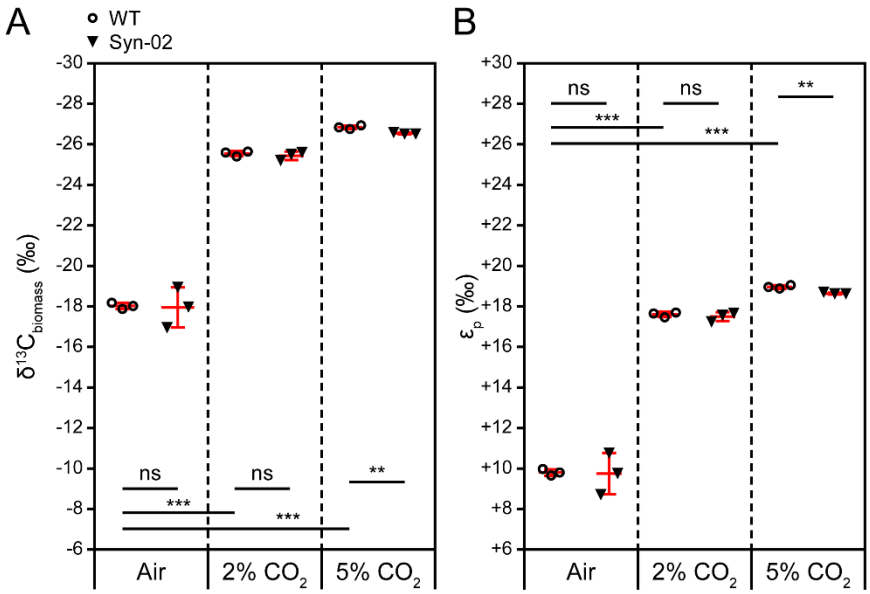

Figure 4. $^{13}C/^{12}C$ discrimination of *S. elongatus* strains under varying CO_2 concentrations. A – Biomass $\delta^{13}C$. Reported $\delta^{13}C$ values are relative to the Vienna PeeDee Belemnite standard (V-PDB). **B – $^{13}C/^{12}C$ discrimination associated with photosynthetic CO_2 fixation (ε_p).** ε_p values are calculated relative to a reference value, $\delta^{13}C_{CO2}$ = -8.4‰ (Keeling et al., 2017) (see **Materials and Methods** for calculation). **A-B –** Mean (middle horizontal bars) and 1 SD (vertical error bars) are shown in red. Asterisks indicate *t*-test results for pairwise comparisons indicated by horizontal lines. ns – not significant; ** – $p < 0.01$; *** – $p < 0.001$.